

A parametric analysis of the seismic performance of bridges as a function of the DCFP device properties

Original

A parametric analysis of the seismic performance of bridges as a function of the DCFP device properties / Castaldo, P.; Amendola, G.. - ELETTRONICO. - II:(2021), pp. 4439-4451. (8th International Conference on Computational Methods in Structural Dynamics and Earthquake Engineering, COMPDYN 2021 grc 2021).

Availability:

This version is available at: 11583/2947856 since: 2021-12-27T09:20:11Z

Publisher:

National Technical University of Athens

Published

DOI:

Terms of use:

This article is made available under terms and conditions as specified in the corresponding bibliographic description in the repository

Publisher copyright

(Article begins on next page)

A PARAMETRIC ANALYSIS OF THE SEISMIC PERFORMANCE OF BRIDGES AS A FUNCTION OF THE DCFP DEVICE PROPERTIES

Paolo Castaldo¹, and Guglielmo Amendola²

¹ Politecnico di Torino, Department of Structural, Geotechnical and Building Engineering (DISEG)
Corso Duca degli Abruzzi 24, 10129, Turin, Italy
e-mail: paolo.castaldo@polito.it

² Politecnico di Torino, Department of Structural, Geotechnical and Building Engineering (DISEG)
Corso Duca degli Abruzzi 24, 10129, Turin, Italy
guglielmo.amendola@polito.it

Abstract

The present investigation examines how the properties of the double concave friction pendulum (DCFP) devices influence the seismic performance of isolated multi-span continuous deck bridges. The numerical simulations are carried out using an eight-degree-of-freedom model to reproduce the elastic behavior of the pier, associated to the assumption of both rigid abutment and rigid deck, and the non-linear velocity-dependent behavior of the two surfaces of the double concave friction pendulum isolators, under a set of natural records with different characteristics. The results in terms of the statistics related to the relevant response parameters are computed in non-dimensional form with respect to the seismic intensity considering different properties of both DCFP isolators and bridge.

Keywords: Seismic isolation, Double concave friction pendulum isolators, Multi-span continuous deck bridges, Performance-based engineering, Non-dimensional form.

1 INTRODUCTION

The seismic isolation is one of the most used and efficient techniques able to improve seismic performance of both new or existing buildings [1]-[2] and infrastructures [3]. With reference to bridges, the seismic isolation allows to uncouple the super-structure represented by the deck and the sub-structure represented by the system piers/abutments/foundations. The main benefit to the structural system relates to significant reduction of forces transmitted from the deck to the piers under seismic event.

In particular, the quantification of safety level of structures [5] and road infrastructures [6]-[8] is a relevant topic for research with special reference to areas subjected to high seismicity. In such areas, the non-linear behaviour of RC members [9]-[11] has a significant influence on structural response when structures are not provided of appropriate isolation systems. For instance, different investigations focused on the analysis of seismic response of bridges equipped with isolator devices have been performed over the years [12].

In literature, several studies have been carried out concerning seismic isolation of bridges through friction pendulum devices (FPS) [13]-[15]. The FPS bearings are able to make the natural period of the isolated bridge independent from the mass of the deck and allows significant energy dissipation under seismic motion thanks to friction on sliding surfaces [16]. The FPS bearings can be realized with single (SCFP) or multiple concave sliding surfaces [17]-[18]. In particular, the use of double concave sliding surface friction pendulum devices (DCFP) have positive influence on the seismic response of isolated bridges as demonstrated by [19].

The present study investigates the effectiveness of the use of DCFP to improve the seismic response of multi-span continuous bridges considering the interaction between piers, abutments and deck [20]. The structural response of the system under seismic excitation is analysed by means of an eight-degree-of-freedom (8-dof) model accounting for the reinforced concrete (RC) pier stiffness, the DCFP behaviour and the rigid RC abutment.

The seismic action and related uncertainties are reproduced adopting a set of natural records having different spectral characteristics. In detail, a non-dimensional parametric study is developed for several geometric configurations of the pier and of the DCFP isolators. The responses of the deck, of the pier and of each surface of the DCFP isolators are monitored to determine effectiveness of the isolation system.

2 DESCRIPTION OF DYNAMIC BEHAVIOUR OF DECK-ABUTMENT-PIER STRUCTURAL SYSTEM

The structural behavior of the multi-span continuous deck bridge (e.g., isolated three-span continuous deck bridge) isolated with DPCF is reproduced by means of an 8-degree-of-freedom (8-dof) system as shown by Figure 1.

In detail, 5 degrees of freedom relate to the lumped masses associated to the RC bridge pier (supposed to be elastic), 2 degrees of freedom correspond to the two sliders of the DPCF bearings and, finally, 1 degree of freedom concerns the mass of the rigid RC deck [14].

The governing equations of motion of the system can be expressed in terms of relative horizontal displacements with respect to the ground (Figure 1(a)) along the longitudinal direction as follows:

$$\begin{aligned}
 m_d [\ddot{u}_d(t) + \ddot{u}_g(t)] + F_{1a}(t) + F_{1p}(t) &= 0 \\
 m_{sa} [\ddot{u}_{sa}(t) + \ddot{u}_g(t)] - F_{1a}(t) + F_{2a}(t) &= 0 \\
 m_{sp} [\ddot{u}_{sp}(t) + \ddot{u}_g(t)] - F_{1p}(t) + F_{2p}(t) &= 0 \quad (1 \text{ a,b,c,d,e}) \\
 m_{p5} [\ddot{u}_{p5}(t) + \ddot{u}_g(t)] + c_{p5} [\dot{u}_{p5}(t) - \dot{u}_{p4}(t)] + k_{p5} [u_{p5}(t) - u_{p4}(t)] - F_{2p}(t) &= 0 \\
 m_{pi} [\ddot{u}_{pi}(t) + \ddot{u}_g(t)] + c_{pi} [\dot{u}_{pi}(t) - \dot{u}_{pi-1}(t)] + k_{pi} [u_{pi}(t) - u_{pi-1}(t)] + \\
 - c_{pi+1} [\dot{u}_{pi+1}(t) - \dot{u}_{pi}(t)] - k_{pi+1} [u_{pi+1}(t) - u_{pi}(t)] &= 0 \quad \text{for } i=1, \dots, 4
 \end{aligned}$$

where u_d denotes the displacement of the deck relative to the ground; u_{sp} is the displacement of the slider of the DCFP device located on the pier with respect to the ground; u_{sa} is the displacement of the slider of the DCFP device located on the abutment with respect to the ground, u_{pi} ($i=1, \dots, 4, 5$) is the displacement relative to the ground of pier i -th mass; m_d , m_{sp} and m_{sa} are the masses of the deck and of the two DCFP devices installed on the pier and on the abutment; m_{pi} ($i=1, \dots, 4, 5$) is the i -th lumped mass of the pier segment; k_{pi} and c_{pi} ($i=1, \dots, 5$) are the stiffness and associated viscous damping constant for each dof associated to the pier segments; t is the time instant; $F_{ja}(t)$ and $F_{jp}(t)$ denote the reaction forces of the DCFP bearings on the abutment and on the pier, respectively, for the upper ($j=1$) and lower sliding surface ($j=2$). With reference to the modelling of behavior of the DCFP, the device can be modelled as a serial combination of two single FPS isolators. Then, according to [17]-[18], the reaction forces at the upper ($j=1$) and lower ($j=2$) surface (i.e., F_1 and F_2) are identical and can be obtained according to the following expression:

$$F = F_1 = F_2 = \frac{m_d g}{R_1 + R_2} (u) + \frac{m_d g (R_1 \mu_1 (\dot{u}_1) \text{sgn}(\dot{u}_1) + R_2 \mu_2 (\dot{u}_2) \text{sgn}(\dot{u}_2))}{R_1 + R_2} \quad (2)$$

where u is the global horizontal displacement of the DCFP isolator; u_1 represents the horizontal displacement of the upper surface ($j=1$); u_2 is the horizontal displacement of the lower surface ($j=2$). The first part of Eq. (2) represents the equivalent restoring stiffness (k_{comb}) of the DCFP device expressed as:

$$k_{comb} = \frac{m_d g}{R_1 + R_2} \quad (3)$$

from which the restoring natural period can be derived as follows:

$$T_d = 2\pi \sqrt{(R_1 + R_2) / g} = 2\pi / \omega_d \quad (4)$$

where g is the gravity constant; R_1 and R_2 denote the upper and lower radius of curvature of the DCFP bearing. In Eq.(2), $\mu_j(\dot{u}_j(t))$ (with $j=1, 2$) represents the sliding friction coefficient, which depends on the slider slip velocity $\dot{u}_j(t)$ along one of the two sliding surfaces and on its sign, $\text{sgn}(\dot{u}_j)$ (for $j=1, 2$). The second part of Eq.(2) represents the equivalent friction coefficient of the DCFP device [17]:

$$\mu_{eqv} = \frac{\mu_1 R_1 + \mu_2 R_2}{R_1 + R_2} \quad (5)$$

Eq.(5) is valid under the assumption that the sliding occurs on the both surfaces of the device and in the same direction.

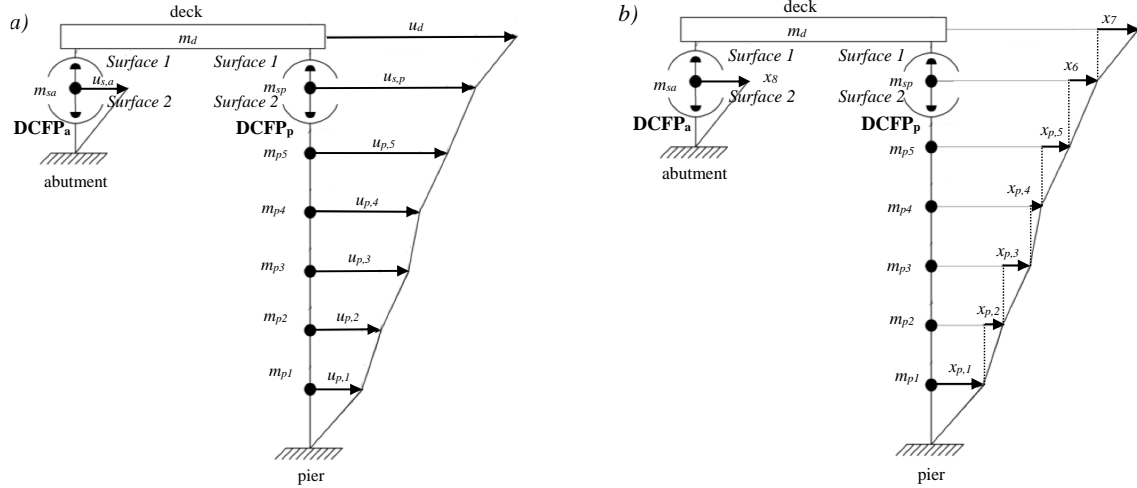


Figure 1: Representation of the 8-dof model of the bridge. Relative displacements with respect to the ground (a) and drifts between the different lumped masses (b).

The experimental investigations of [21]-[23] demonstrate that, the coefficient of friction on sliding surfaces of DCFP can be estimated according to the following expression:

$$\mu_j(\dot{u}_j) = \mu_{j,\max} - (\mu_{j,\max} - \mu_{j,\min}) \cdot \exp(-\alpha |\dot{u}_j|) \quad \text{for } j = 1, 2 \quad (6)$$

where, $\mu_{j,\max}$ denotes the maximum value of friction coefficient at high sliding velocities; $\mu_{j,\min}$ represents the value at near-zero sliding velocity. In the present investigation, it is assumed that $\mu_{j,\max} = 3\mu_{j,\min}$ and $\alpha = 30$ according to the researches of [21]-[23].

3 NON-DIMENSIONAL SYSTEM OF EQUATIONS

The analysis of the seismic behavior of the bridge under seismic action is performed according to non-dimensional form of the system of equations of motion, in line with previous applications [24]. In order to obtain the response of the DCFP devices along each sliding surface, Eq.(1) can be expressed in terms of drifts between the lumped masses of the structural system (Fig.1(b)), according to the following relationships:

$$\begin{aligned} & m_d \ddot{x}_7(t) + m_d \ddot{x}_6(t) + m_d \ddot{x}_{p5}(t) + m_d \ddot{x}_{p4}(t) + m_d \ddot{x}_{p3}(t) + m_d \ddot{x}_{p2}(t) + m_d \ddot{x}_{p1}(t) + \\ & + c_d \dot{x}_d(t) + F_{1a}(t) + F_{1p}(t) = -m_d \ddot{u}_g(t) \\ & m_{sp} \ddot{x}_6(t) + m_{sp} \ddot{x}_{p5}(t) + m_{sp} \ddot{x}_{p4}(t) + m_{sp} \ddot{x}_{p3}(t) + m_{sp} \ddot{x}_{p2}(t) + m_{sp} \ddot{x}_{p1}(t) - F_{1p}(t) + F_{2p}(t) = -m_{sp} \ddot{u}_g(t) \\ & m_{sa} \ddot{x}_8(t) - F_{1a}(t) + F_{2a}(t) = -m_{sa} \ddot{u}_g(t) \\ & m_{p5} \ddot{x}_{p5}(t) + m_{p5} \ddot{x}_{p4}(t) + m_{p5} \ddot{x}_{p3}(t) + m_{p5} \ddot{x}_{p2}(t) + m_{p5} \ddot{x}_{p1}(t) - c_d \dot{x}_d(t) + c_{p5} \dot{x}_{p5}(t) + \\ & + k_{p5} x_{p5}(t) - F_{2p}(t) = -m_{p5} \ddot{u}_g(t) \\ & m_{p4} \ddot{x}_{p4}(t) + m_{p4} \ddot{x}_{p3}(t) + m_{p4} \ddot{x}_{p2}(t) + m_{p4} \ddot{x}_{p1}(t) - c_{p5} \dot{x}_{p5}(t) - k_{p5} x_{p5}(t) + c_{p4} \dot{x}_{p4}(t) + k_{p4} x_{p4}(t) = -m_{p4} \ddot{u}_g(t) \\ & m_{p3} \ddot{x}_{p3}(t) + m_{p3} \ddot{x}_{p2}(t) + m_{p3} \ddot{x}_{p1}(t) - c_{p4} \dot{x}_{p4}(t) - k_{p4} x_{p4}(t) + c_{p3} \dot{x}_{p3}(t) + k_{p3} x_{p3}(t) = -m_{p3} \ddot{u}_g(t) \\ & m_{p2} \ddot{x}_{p2}(t) + m_{p2} \ddot{x}_{p1}(t) - c_{p3} \dot{x}_{p3}(t) - k_{p3} x_{p3}(t) + c_{p2} \dot{x}_{p2}(t) + k_{p2} x_{p2}(t) = -m_{p2} \ddot{u}_g(t) \\ & m_{p1} \ddot{x}_{p1}(t) - c_{p2} \dot{x}_{p2}(t) - k_{p2} x_{p2}(t) + c_{p1} \dot{x}_{p1}(t) + k_{p1} x_{p1}(t) = -m_{p1} \ddot{u}_g(t) \end{aligned} \quad (7a,b,c,d,e,f,g,h)$$

where, in line to Eq.s(2)-(6), the reactions of the DCFP bearings on the sliding surfaces are:

$$\begin{aligned}
 F_{1a} &= \frac{m_d g}{2} \left[\frac{1}{R_{1a}} \left(\sum_{i=1}^5 x_{pi} + x_6 + x_7 - x_8 \right) + \mu_{1a}(\dot{x}_9) (\text{sgn}(\dot{x}_9)) \right] \\
 F_{2a} &= \left(\frac{m_d}{2} + m_{sa} \right) g \left[\frac{1}{R_{2a}} (x_8) + (\mu_{2a}(\dot{x}_8)) (\text{sgn}(\dot{x}_8)) \right] \\
 F_{1p} &= \left(\frac{m_d g}{2} \right) \left[\frac{1}{R_{1p}} (x_7) + (\mu_{1p}(\dot{x}_7)) (\text{sgn}(\dot{x}_7)) \right] \\
 F_{2p} &= \left(\frac{m_d}{2} + m_{sp} \right) g \left[\frac{1}{R_{2p}} (x_6) + (\mu_{2p}(\dot{x}_6)) (\text{sgn}(\dot{x}_6)) \right]
 \end{aligned} \tag{8 a,b,c,d}$$

where, in detail, $x_9 = u_d - x_8 = \sum_{i=1}^5 x_{pi} + x_6 + x_7 - x_8$. Next, dividing all the equations by the mass m_d , the system of equation of Eq.(7) becomes:

$$\begin{aligned}
 &\ddot{x}_7(t) + \ddot{x}_6(t) + \ddot{x}_{p5}(t) + \ddot{x}_{p4}(t) + \ddot{x}_{p3}(t) + \ddot{x}_{p2}(t) + \ddot{x}_{p1}(t) + 2\xi_d \omega_d \dot{x}_d(t) + \\
 &+ \frac{g}{2} \left[\frac{1}{R_{1a}} \left(\sum_{i=1}^5 x_{pi} + x_6 + x_7 - x_8 \right) + \mu_{1a}(v) \left(\text{sgn} \left(\sum_{i=1}^5 \dot{x}_{pi} + \dot{x}_6 + \dot{x}_7 - \dot{x}_8 = v \right) \right) \right] + \\
 &+ \frac{g}{2} \left[\frac{1}{R_{1p}} (x_7) + (\mu_{1p}(\dot{x}_7)) (\text{sgn}(\dot{x}_7)) \right] = \ddot{u}_g(t) \\
 \\
 &\lambda_{sp} (\ddot{x}_6(t) + \ddot{x}_{p5}(t) + \ddot{x}_{p4}(t) + \ddot{x}_{p3}(t) + \ddot{x}_{p2}(t) + \ddot{x}_{p1}(t)) + \\
 &- \frac{g}{2} \left[\frac{1}{R_{1p}} (x_7) + (\mu_{1p}(\dot{x}_7)) (\text{sgn}(\dot{x}_7)) \right] + \left(\frac{1}{2} + \lambda_{sp} \right) g \left[\frac{1}{R_{2p}} (x_6) + (\mu_{2p}(\dot{x}_6)) (\text{sgn}(\dot{x}_6)) \right] = -\lambda_{sp} \ddot{u}_g(t) \\
 \\
 &\lambda_{sa} \ddot{x}_8(t) - \frac{g}{2} \left[\frac{1}{R_{1a}} \left(\sum_{i=1}^5 x_{pi} + x_6 + x_7 - x_8 \right) + \mu_{1a}(v) \left(\text{sgn} \left(\sum_{i=1}^5 \dot{x}_{pi} + \dot{x}_6 + \dot{x}_7 - \dot{x}_8 = v \right) \right) \right] + \\
 &+ \left(\frac{1}{2} + \lambda_{sa} \right) g \left[\frac{1}{R_{2a}} (x_8) + (\mu_{2a}(\dot{x}_8)) (\text{sgn}(\dot{x}_8)) \right] = -\lambda_{sa} \ddot{u}_g(t) \\
 \\
 &\lambda_{p5} (\ddot{x}_{p5}(t) + \ddot{x}_{p4}(t) + \ddot{x}_{p3}(t) + \ddot{x}_{p2}(t) + \ddot{x}_{p1}(t)) - 2\xi_d \omega_d \dot{x}_d(t) + 2\xi_{p5} \omega_{p5} \lambda_{p5} \dot{x}_{p5}(t) + \omega_{p5}^2 \lambda_{p5} x_{p5}(t) + \\
 &- \left(\frac{1}{2} + \lambda_{sp} \right) g \left[\frac{1}{R_{2p}} (x_6) + (\mu_{2p}(\dot{x}_6)) (\text{sgn}(\dot{x}_6)) \right] = -\lambda_{p5} \ddot{u}_g(t)
 \end{aligned} \tag{9a,b,c,d,e,f,g,h}$$

$$\begin{aligned}
 &\lambda_{p4} (\ddot{x}_{p4}(t) + \ddot{x}_{p3}(t) + \ddot{x}_{p2}(t) + \ddot{x}_{p1}(t)) - 2\xi_{p5} \omega_{p5} \lambda_{p5} \dot{x}_{p5}(t) - \omega_{p5}^2 \lambda_{p5} x_{p5}(t) + \\
 &+ 2\xi_{p4} \omega_{p4} \lambda_{p4} \dot{x}_{p4}(t) + \omega_{p4}^2 \lambda_{p4} x_{p4}(t) = -\lambda_{p4} \ddot{u}_g(t) \\
 &\lambda_{p3} (\ddot{x}_{p3}(t) + \ddot{x}_{p2}(t) + \ddot{x}_{p1}(t)) - 2\xi_{p4} \omega_{p4} \lambda_{p4} \dot{x}_{p4}(t) - \omega_{p4}^2 \lambda_{p4} x_{p4}(t) + 2\xi_{p3} \omega_{p3} \lambda_{p3} \dot{x}_{p3}(t) + \omega_{p3}^2 \lambda_{p3} x_{p3}(t) = -\lambda_{p3} \ddot{u}_g(t) \\
 &\lambda_{p2} (\ddot{x}_{p2}(t) + \ddot{x}_{p1}(t)) - 2\xi_{p3} \omega_{p3} \lambda_{p3} \dot{x}_{p3}(t) - \omega_{p3}^2 \lambda_{p3} x_{p3}(t) + 2\xi_{p2} \omega_{p2} \lambda_{p2} \dot{x}_{p2}(t) + \omega_{p2}^2 \lambda_{p2} x_{p2}(t) = -\lambda_{p2} \ddot{u}_g(t) \\
 &\lambda_{p1} \ddot{x}_{p1}(t) - 2\xi_{p2} \omega_{p2} \lambda_{p2} \dot{x}_{p2}(t) - \omega_{p2}^2 \lambda_{p2} x_{p2}(t) + 2\xi_{p1} \omega_{p1} \lambda_{p1} \dot{x}_{p1}(t) + \omega_{p1}^2 \lambda_{p1} x_{p1}(t) = -\lambda_{p1} \ddot{u}_g(t)
 \end{aligned}$$

introducing the mass ratios; the circular frequency of vibration of the isolated deck and of the i -th dof of the pier; the damping coefficient of the i -th dof of the pier, as expressed in the following:

$$\lambda_{pi} = \frac{m_{pi}}{m_d}, \quad \lambda_{sa} = \frac{m_{sa}}{m_d}, \quad \lambda_{sp} = \frac{m_{sp}}{m_d}, \quad \omega_d = \sqrt{\frac{k_{comb}}{m_d}}, \quad \omega_{pi} = \sqrt{\frac{k_{pi}}{m_{pi}}}, \quad \xi_{pi} = \frac{c_{pi}}{2m_{pi}\omega_{pi}} \tag{10 a,b,c,d,e,f}$$

In line to [24], the time scale $\tau = t\omega_d$ can be introduced together with the seismic intensity scale factor a_0 , expressed as $\ddot{u}_g(t) = a_0 \ell(\tau)$. The function $\ell(\tau)$ is a non-dimensional function of

time describing the time history of the seismic input. Finally, the non-dimensional system equations can be expressed as follows:

$$\begin{aligned}
 & \ddot{\psi}_7(\tau) + \ddot{\psi}_6(\tau) + \ddot{\psi}_{p5}(\tau) + \ddot{\psi}_{p4}(\tau) + \ddot{\psi}_{p3}(\tau) + \ddot{\psi}_{p2}(\tau) + \ddot{\psi}_{p1}(\tau) + 2\xi_d \dot{\psi}_7(\tau) + \frac{g}{2} \left[\frac{1}{R_{1p}} \frac{1}{\omega_d^2} \psi_7(\tau) + \frac{\mu_{1p}(\dot{\psi}_7)}{a_0} \text{sgn}(\dot{\psi}_7) \right] + \\
 & + \frac{g}{2} \left[\frac{1}{R_{1a}} \frac{1}{\omega_d^2} \left(\sum_{i=1}^5 \psi_{pi}(\tau) + \psi_6(\tau) + \psi_7(\tau) - \psi_8(\tau) \right) + \left(\frac{\mu_{1a}(\dot{\psi}_9)}{a_0} \right) \left(\text{sgn} \left(\sum_{i=1}^5 \dot{\psi}_{pi}(\tau) + \dot{\psi}_6(\tau) + \dot{\psi}_7(\tau) - \dot{\psi}_8(\tau) \right) \right) \right] = -\ell(\tau) \\
 \\
 & \lambda_{sp} \left[\ddot{\psi}_6(\tau) + \ddot{\psi}_{p5}(\tau) + \ddot{\psi}_{p4}(\tau) + \ddot{\psi}_{p3}(\tau) + \ddot{\psi}_{p2}(\tau) + \ddot{\psi}_{p1}(\tau) \right] - \frac{g}{2} \left[\frac{1}{R_{1p}} \frac{1}{\omega_d^2} \psi_7(\tau) + \frac{\mu_{1p}(\dot{\psi}_7)}{a_0} \text{sgn}(\dot{\psi}_7) \right] + \\
 & + \left(\frac{1}{2} + \lambda_{sp} \right) g \left[\frac{1}{R_{2p}} \frac{1}{\omega_d^2} \psi_6(\tau) + \frac{\mu_{2p}(\dot{\psi}_6)}{a_0} \text{sgn}(\dot{\psi}_6) \right] = -\lambda_{sp} \ell(\tau) \\
 \\
 & \lambda_{sa} \ddot{\psi}_8(\tau) - \frac{g}{2} \left[\frac{1}{R_{1a}} \frac{1}{\omega_d^2} \left(\sum_{i=1}^5 \psi_{pi}(\tau) + \psi_6(\tau) + \psi_7(\tau) - \psi_8(\tau) \right) + \left(\frac{\mu_{1a}(\dot{\psi}_9)}{a_0} \right) \left(\text{sgn} \left(\sum_{i=1}^5 \dot{\psi}_{pi}(\tau) + \dot{\psi}_6(\tau) + \dot{\psi}_7(\tau) - \dot{\psi}_8(\tau) \right) \right) \right] + \\
 & + \left(\frac{1}{2} + \lambda_{sa} \right) g \left[\frac{1}{R_{2a}} \frac{1}{\omega_d^2} \psi_8(\tau) + \frac{\mu_{2a}(\dot{\psi}_8)}{a_0} \text{sgn}(\dot{\psi}_8) \right] = -\lambda_{sa} \ell(\tau) \\
 \\
 & \lambda_{p5} \left[\ddot{\psi}_{p5}(\tau) + \ddot{\psi}_{p4}(\tau) + \ddot{\psi}_{p3}(\tau) + \ddot{\psi}_{p2}(\tau) + \ddot{\psi}_{p1}(\tau) \right] - 2\xi_d \dot{\psi}_d(\tau) + 2\xi_{p5} \lambda_{p5} \frac{\omega_{p5}}{\omega_d} \dot{\psi}_{p5}(\tau) + \frac{\lambda_{p5} \omega_{p5}^2}{\omega_d^2} \psi_{p5}(\tau) + \\
 & - \left(\frac{1}{2} + \lambda_{sp} \right) g \left[\frac{1}{R_{2p}} \frac{1}{\omega_d^2} \psi_6(\tau) + \frac{\mu_{2p}(\dot{\psi}_6)}{a_0} \text{sgn}(\dot{\psi}_6) \right] = -\lambda_{p5} \ell(\tau) \\
 \\
 & \lambda_{p4} \left[\ddot{\psi}_{p4}(\tau) + \ddot{\psi}_{p3}(\tau) + \ddot{\psi}_{p2}(\tau) + \ddot{\psi}_{p1}(\tau) \right] - 2\xi_{p5} \lambda_{p5} \frac{\omega_{p5}}{\omega_d} \dot{\psi}_{p5}(\tau) + \\
 & + 2\xi_{p4} \lambda_{p4} \frac{\omega_{p4}}{\omega_d} \dot{\psi}_{p4}(\tau) - \lambda_{p5} \frac{\omega_{p5}^2}{\omega_d^2} \psi_{p5}(\tau) + \lambda_{p4} \frac{\omega_{p4}^2}{\omega_d^2} \psi_{p4}(\tau) = -\lambda_{p4} \ell(\tau) \\
 \\
 & \lambda_{p3} \left[\ddot{\psi}_{p3}(\tau) + \ddot{\psi}_{p2}(\tau) + \ddot{\psi}_{p1}(\tau) \right] - 2\xi_{p4} \lambda_{p4} \frac{\omega_{p4}}{\omega_d} \dot{\psi}_{p4}(\tau) + \\
 & + 2\xi_{p3} \lambda_{p3} \frac{\omega_{p3}}{\omega_d} \dot{\psi}_{p3}(\tau) - \lambda_{p4} \frac{\omega_{p4}^2}{\omega_d^2} \psi_{p4}(\tau) + \lambda_{p3} \frac{\omega_{p3}^2}{\omega_d^2} \psi_{p3}(\tau) = -\lambda_{p3} \ell(\tau) \\
 \\
 & \lambda_{p2} \left[\ddot{\psi}_{p2}(\tau) + \ddot{\psi}_{p1}(\tau) \right] - 2\xi_{p3} \lambda_{p3} \frac{\omega_{p3}}{\omega_d} \dot{\psi}_{p3}(\tau) + 2\xi_{p2} \lambda_{p2} \frac{\omega_{p2}}{\omega_d} \dot{\psi}_{p2}(\tau) - \lambda_{p3} \frac{\omega_{p3}^2}{\omega_d^2} \psi_{p3}(\tau) + \\
 & + \lambda_{p2} \frac{\omega_{p2}^2}{\omega_d^2} \psi_{p2}(\tau) = -\lambda_{p2} \ell(\tau) \\
 \\
 & \lambda_{p1} \ddot{\psi}_{p1}(\tau) - 2\xi_{p2} \lambda_{p2} \frac{\omega_{p2}}{\omega_d} \dot{\psi}_{p2}(\tau) + 2\xi_{p1} \lambda_{p1} \frac{\omega_{p1}}{\omega_d} \dot{\psi}_{p1}(\tau) - \lambda_{p2} \frac{\omega_{p2}^2}{\omega_d^2} \psi_{p2}(\tau) + \lambda_{p1} \frac{\omega_{p1}^2}{\omega_d^2} \psi_{p1}(\tau) = -\lambda_{p1} \ell(\tau)
 \end{aligned}$$

(11 a,b,c,d,e,f,g,h)

with the following non-dimensional parameters:

$$\begin{aligned}
 \Pi_{oi} &= \frac{\omega_{pi}}{\omega_d} \quad , \quad \Pi_{\lambda_i} = \lambda_{pi} = \frac{m_{pi}}{m_d} \quad , \quad \Pi_{\lambda_{sa}} = \lambda_{sa} \quad , \\
 \Pi_{\lambda_{sp}} &= \lambda_{sp} \quad , \quad \Pi_{\mu_{1a}}(\dot{\psi}_9) = \frac{\mu_{1a}(\dot{\psi}_9) g}{a_0} \quad , \\
 \Pi_{\mu_{1p}}(\dot{\psi}_7) &= \frac{\mu_{1p}(\dot{\psi}_7) g}{a_0} \quad , \quad \Pi_{\mu_{2a}}(\dot{\psi}_8) = \frac{\mu_{2a}(\dot{\psi}_8) g}{a_0} \quad , \\
 \Pi_{\mu_{2p}}(\dot{\psi}_6) &= \frac{\mu_{2p}(\dot{\psi}_6) g}{a_0} \quad , \quad \Pi_{\xi_{pi}} = \xi_{pi}
 \end{aligned}$$

(12 a,b,c,d,e,f,g,h,i)

The non-dimensional parameters $\Pi_{\mu_{1a}}, \Pi_{\mu_{1p}}, \Pi_{\mu_{2a}}, \Pi_{\mu_{2p}}$ depend from the velocities and are used as follows:

$$\Pi_{\mu_{1a}}^* = \frac{\mu_{1,\max,a} g}{a_0}, \quad \Pi_{\mu_{1p}}^* = \frac{\mu_{1,\max,p} g}{a_0}, \quad \Pi_{\mu_{2a}}^* = \frac{\mu_{2,\max,a} g}{a_0}, \quad \Pi_{\mu_{2p}}^* = \frac{\mu_{2,\max,p} g}{a_0} \quad (13 \text{ a,b,c,d})$$

With reference to Figure 1, it can be recognized that the peak response in terms of non-dimensional parameters can be expressed as:

$$\psi_{u_d} = \frac{u_{d,\text{peak}} \omega_d^2}{a_0}, \quad \psi_{x_d} = \frac{x_{d,\text{peak}} \omega_d^2}{a_0} = \frac{(x_6 + x_7)_{\text{peak}} \omega_d^2}{a_0}, \quad \psi_{u_p} = \frac{u_{p,\text{peak}} \omega_d^2}{a_0} = \frac{\left(\sum_{i=1}^5 x_i \right)_{\text{peak}} \omega_d^2}{a_0} \quad (14 \text{ a,b,c})$$

4 PARAMETRIC INVESTIGATION OF STRUCTURAL RESPONSE UNDER SEISMIC ACTIONS

Next, the results of parametric analysis of the bridge system isolated with DCFP bearings of Figure 1 are reported in non-dimensional terms. Firstly, the criteria for selection of earthquake events and the response parameters adopted to monitor the seismic performance are described.

4.1 Selection of the seismic inputs

In line with the approach of performance-based earthquake engineering (PBEE) [25], the present investigation accounts for the uncertainties related to the seismic input intensity separately from the ones related to the characteristics of the record (i.e., record-to-record variability). This is possible to the introduction of an intensity measure (IM) that corresponds to the seismic intensity scale factor a_0 . According to the criteria of efficiency, sufficiency and hazard compatibility [26], this study assumes that the spectral pseudo-acceleration, S_A , at the isolated period of the system, $T_d = 2\pi / \omega_d$ (Eq.(4)), represents the adopted intensity measure IM. In the parametric analyses, ξ_d is taken equal to zero, in line to [24]. Then, the related $IM = a_0$ is hereinafter denoted to as $S_A(T_d)$. The record-to-record variability is described through a set of 30 ground motion records with details in [27]-[30].

4.2 Evaluation of the seismic response

In the present investigation, the peak response parameters considered are the following:

- the *peak deck response* $u_{d,\text{peak}}$, that corresponds to the peak isolator global response on the abutment;
- the *peak isolator global response* on the pier, $x_{d,\text{peak}}$;
- the *peak displacement at the top of the pier* $u_{p,\text{peak}}$ with respect to the ground.

According to the nondimensionalization previously introduced, the solution of Eq. (11) for the ground motions records allows to determine a set of samples of the mentioned above output variables. Next, the non-dimensional response parameters are assumed consistent with a lognormal probabilistic model as widely employed in PBEE [31] and in other studies [32]-[39]. The statistical parameters for lognormal distribution can be derived from generic response parameter D (i.e., the extreme values of ψ_{u_d} , ψ_{x_p} and ψ_{u_p} of Eq.s (11) and (14)) by estimating the mean value $GM(D)$ and the coefficient of variation $\beta(D)$ of the observed samples as follows:

$$GM(D) = \sqrt[N]{d_1 \cdot \dots \cdot d_N} \quad (15)$$

$$\beta(D) = \sqrt{\frac{(\ln d_1 - \ln[GM(D)])^2 + \dots + (\ln d_N - \ln[GM(D)])^2}{N-1}} \quad (16)$$

where d_h represents the h -th sample value of D associated to the h -th accelerogram and N is the total number of samples equal to the total number of accelerograms herein adopted ($h=1, \dots, N$). According to the lognormal distribution assumption, the k -th percentile of the generic response parameter D can be derived as follows:

$$d_k = GM(D) \exp[f(k)\beta(D)] \quad (17)$$

where $f(k)$ assume the values of $f(50) = 0$ for 50-th percentile and $f(84) = 1$ for 84-percentile, respectively [40].

4.3 Outcomes from non-dimensional analyses

This section reports the results of the parametric investigation developed in line to the proposed criteria for nondimensionalization of the equations of motion. The influence of the properties of the DCFP isolators and bridge geometry on the seismic performance of the structural system under the ground motion records has been investigated. The following parametric analysis has been carried out:

- the parameters $\Pi_{\xi_d} = \xi_d$ and $\Pi_{\xi_p} = \xi_p$ are assumed equal to 0% and 5%;
- the isolated bridge period T_d has been assumed as 2s, 2.5s, 3s, 3.5s and 4s;
- the RC pier period T_p equal to 0.2s [19];
- the five pier lumped masses $\Pi_{\lambda} = \lambda_p$ has been considered equal to 0.1, 0.15 and 0.2 [19];
- the two DCFP devices on the abutment and on the pier have identical properties (i.e., follows that $\Pi_{\mu_{1a}}^* = \Pi_{\mu_{1p}}^* = \Pi_{\mu_1}^*$ as well as $\Pi_{\lambda_{sa}} = \Pi_{\lambda_{sp}} = \Pi_{\lambda_s}$) and the mass ratio Π_{λ_s} is set equal to 0.005; R_1 / R_2 equal to 2, $\mu_{1,\max} / \mu_{2,\max}$ equal to 4, $\mu_{j,\max} / \mu_{j,\min}$ (with $j=1,2$) equal to 3;
- the parameter $\Pi_{\mu_1}^*$ is assumed to vary in the range between 0 (no friction) and 2 (very high friction) (specifically, 95 values are considered).

Then, the non-dimensional parametric investigations have been carried out on 1425 different systems, defined by varying the main structural properties within the two bearing cases, assuming 30 different ground motions. For each value of the parameters of interest in the parametric study, the differential equations of motion, (i.e., Eq. (11)), have been solved for the 30 different ground motions. The Bogacki-Shampine integration algorithm available in Matlab-Simulink [41] has been adopted.

Fig.s 2-4 show the statistics (GM and β values) of the non-dimensional peak response parameters considered, obtained for different values of the system properties varying in the range of interest. Each figure contains three surface plots, corresponding to the different values of Π_{λ} .

Fig. 2 plots the results concerning the peak normalized displacement of pier top ψ_{u_p} with respect to the ground. It is noteworthy that for very low $\Pi_{\mu_1}^*$ values, $GM(\psi_{u_p})$ decreases by increasing $\Pi_{\mu_1}^*$, whereas it increases for high $\Pi_{\mu_1}^*$ values. Thus, there exists an optimal value

of $\Pi_{\mu 1}^*$ such that the peak displacement of pier top is minimized. This optimal value varies between 0 and 0.5 depending on the values of T_d and Π_λ . In addition, $GM(\psi_{u_p})$ decreases significantly with increasing Π_λ . The parameter T_d has an influence on $GM(\psi_{u_p})$ leading to a general decrease for an its increase thanks to the effectiveness of the seismic isolation. The dispersion $\beta(\psi_{u_p})$ shows a maximum value approximatively at the same value of $\Pi_{\mu 1}^*$ that gives the minimum $GM(\psi_{u_p})$. The response dispersion increases with increasing the mass ratio Π_λ . From low to high values of T_d , $\beta(\psi_{u_p})$ also increases.

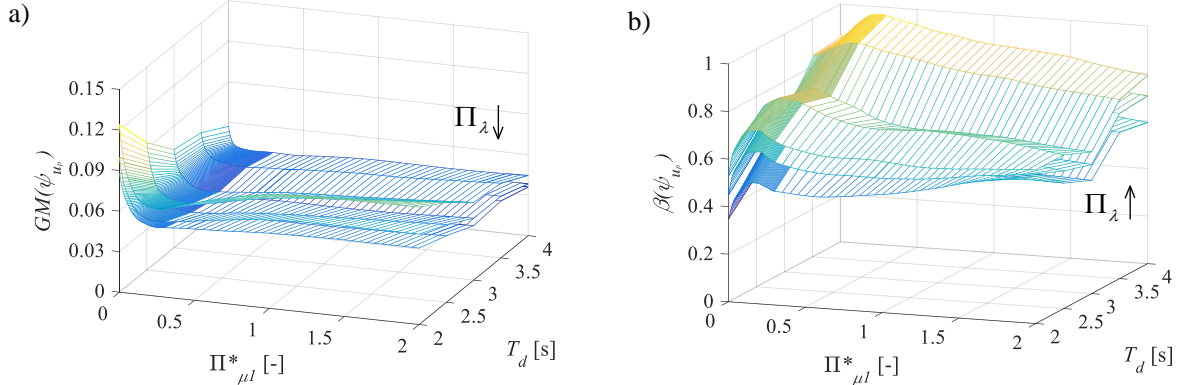


Figure 2: Normalized displacement of pier top vs. $\Pi_{\mu 1}^*$ and T_d : median value and dispersion for $T_p = 0.2s$ and for different values of Π_λ . The arrow denotes the increasing direction of Π_λ .

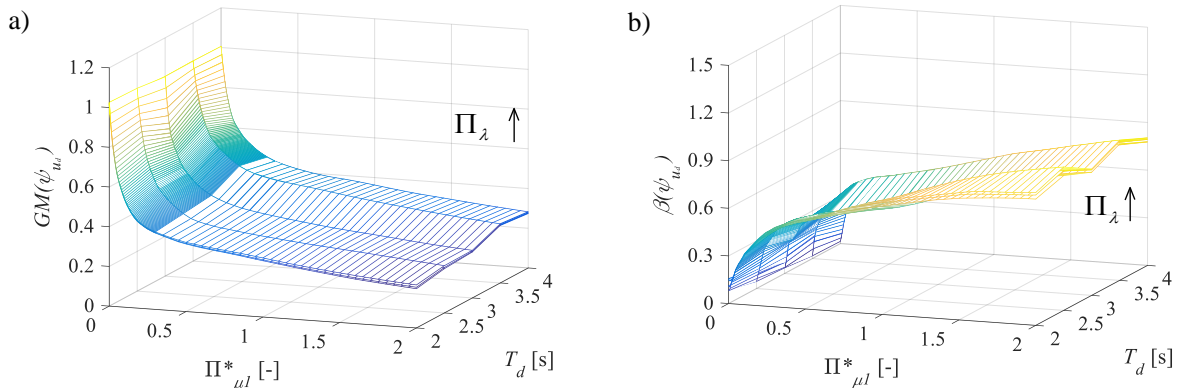


Figure 3. Normalized deck displacement vs. $\Pi_{\mu 1}^*$ and T_d : median value and dispersion for $T_p = 0.2s$ and for different values of Π_λ . The arrow denotes the increasing direction of Π_λ .

Fig. 3 shows the response statistics of the peak normalized deck displacement ψ_{u_d} , which also corresponds to the peak global response of the bearing placed on the abutment. Obviously, $GM(\psi_{u_d})$ decreases significantly as $\Pi_{\mu 1}^*$ increases. In general, the values of $GM(\psi_{u_d})$ slightly increase for increasing values of both T_d and Π_λ . The values of the dispersion $\beta(\psi_{u_d})$, plotted in Fig. 3 (b), are very low for low $\Pi_{\mu 1}^*$ values due to the high efficiency of the *IM*, and attain their maximum for high values of $\Pi_{\mu 1}^*$. The other system properties have a reduced influence on $\beta(\psi_{u_d})$ compared to the influence of $\Pi_{\mu 1}^*$.

Fig. 4 shows the variation of the peak global response with regard to the bearing placed on the pier ψ_{x_d} . As already observed for $GM(\psi_{u_d})$, also $GM(\psi_{x_d})$ tends to show a decrease

against increasing $\Pi_{\mu 1}^*$ values. The dispersion is low in correspondence of low $\Pi_{\mu 1}^*$ values due to the high efficiency of the *IM*, attaining its peak for high $\Pi_{\mu 1}^*$ values. Note that the influence of Π_{λ} is slightly more marked for $GM(\psi_{x_d})$ with respect to $GM(\psi_{u_d})$ leading to lower values due to the flexibility of the pier.

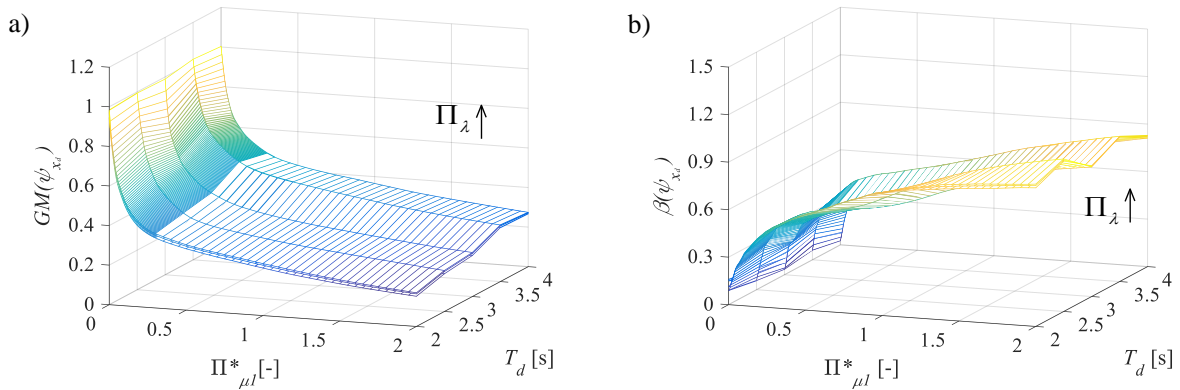


Figure 4. Normalized pier bearing global displacement vs. $\Pi_{\mu 1}^*$ and T_d : median value and dispersion for $T_p = 0.2s$ and for different values of Π_{λ} . The arrow denotes the increasing direction of Π_{λ} .

The existence of an optimal value of the normalised friction coefficient of the upper surface $\Pi_{\mu 1}^*$ for the both DCFP devices able to minimize the displacement of pier top (Fig. 2) is the result of counteracting effects that occur for increasing values of the friction coefficient.

5 CONCLUSIONS

This paper analyzes the seismic performance of multi-span continuous deck bridges isolated with DCFP devices considering the pier-abutment-deck interaction. The results of an extensive non-dimensional parametric study encompassing a wide range of isolator and bridge properties have been illustrated monitoring various response parameters of interest related to both the isolators and the pier. Specifically, the RC pier is considered elastic, whereas the RC deck and RC abutment are assumed rigid. The results in terms of geometric mean and dispersion for each peak normalised response parameter are summarized as follows.

Regarding the pier performance, there exists an optimal value of sliding friction coefficient for each surface of the DCFP device able to minimize the pier response. This optimal value depends on the bridge and isolator properties.

Regarding the deck performance, which also corresponds to the peak global response of the bearing placed on the abutment, the response decreases significantly as the sliding friction coefficient increases. Slightly lower results are achieved for the global response of the bearing placed on the pier.

REFERENCES

- [1] D. Gino, P. Castaldo, C. Anerdi, M. Ferrara, G. Bertagnoli, L. Giordano, Seismic upgrading of existing reinforced concrete buildings using friction pendulum Devices: A Probabilistic Evaluation. *Applied Sciences*, **10**, 8980, 2020, doi:10.3390/app10248980

- [2] P. Castaldo, G. Alfano, Seismic reliability-based design of hardening and softening structures isolated by double concave sliding devices. *Soil Dynamics and Earthquake Engineering*, **129**, 105930, 2020.
- [3] M.C. Constantinou, A. Kartoum, A.M. Reinhorn, P. Bradford, Sliding isolation system for bridges. *Experimental study, Earthquake Spectra* **8**(3), 321-344, 1992.
- [4] A. Ghobarah, H.M. Ali, Seismic performance of highway bridges. *Eng. Struct.*, **10**(3): 157-166, 1988.
- [5] G. Mancini, V.I. Carbone, G. Bertagnoli, D. Gino, Reliability-based evaluation of bond strength for tensed lapped joints and anchorages in new and existing reinforced concrete structures. *Structural Concrete*, **19**(3), 904-917, 2018. <https://doi.org/10.1002/suco.201700082>
- [6] D. Gino, P. Castaldo, G. Bertagnoli, L. Giordano, G. Mancini, Partial factor methods for existing structures according to fib Bulletin 80: Assessment of an existing prestressed concrete bridge. *Structural Concrete*, **21**, 15-31, 2020, <https://doi.org/10.1002/suco.201900231>.
- [7] Troisi R., Alfano G. 2019. Towns as Safety Organizational Fields: An Institutional Framework in Times of Emergency. *Sustainability*, **11**: 7025, 2019, doi:10.3390/su11247025.
- [8] Troisi R., Alfano G. 2020. Firms' crimes and land use in Italy. An exploratory data analysis. New Metropolitan Perspectives, International Symposium – 4th edition, 27-30 May 2020, pp 10.
- [9] D. Gino, G. Bertagnoli, D. La Mazza, G. Mancini, A quantification of model uncertainties in NLFEA of R.C. shear walls subjected to repeated loading, *Ingegneria Sismica (International journal of earthquake engineering)*, **34**(3-4), 79-91, 2017.
- [10] D. Gino, P. Castaldo, L. Giordano, G. Mancini, Model uncertainty in non-linear numerical analyses of slender reinforced concrete members. *Structural Concrete*, 1–26, 2021, <https://doi.org/10.1002/suco.202000600>.
- [11] G. Bertagnoli, D. Gino, E. Martinelli, A simplified method for predicting early-age stresses in slabs of steel-concrete composite beams in partial interaction. *Engineering Structures*, **14**, 286-297, 2017, 10.1016/j.engstruct.2017.02.058.
- [12] P. Tsopelas, M.C. Constantinou, S. Okamoto, S. Fujii, D. Ozaki, Experimental study of bridge seismic sliding isolation systems. *Eng. Struct.*, **18**(4), 301-310, 1996.
- [13] B.A. Olmos, J.M. Jara, J.M. Roesset, Effects of isolation on the seismic response of bridges designed for two different soil types. *Bulletin of Earthquake Engineering*, **9**(2), 641-656, 2011.
- [14] R.S. Jangid, Stochastic Response of Bridges Seismically Isolated by Friction Pendulum System. *J. Bridge Eng.*, **13**(4), 319, 2008.
- [15] M. Dicleli, S. Buddaram, Effect of isolator and ground motion characteristics on the performance of seismic - isolated bridges. *Earthquake engineering & structural dynamics*, **35**(2), 233-250, 2006.
- [16] V.A. Zayas, S.S. Low, S.A. Mahin, A simple pendulum technique for achieving seismic isolation. *Earthquake Spectra*, **6**, 317–33, 1990.

- [17] D.M. Fenz, M.C. Constantinou, Behaviour of the double concave friction pendulum bearing. *Earthquake Engineering and Structural Dynamics*, **35**:1403-1424, 2006.
- [18] M.C. Constantinou, Friction pendulum double concave bearings. *technical report University of Buffalo NY*, October 29, 2004.
- [19] Y.S. Kim, C.B. Yun, Seismic response characteristics of bridges using double concave friction pendulum bearings with tri-linear behavior. *Engin. Struct.*, **29**, 3082-3093, 2007.
- [20] M.C. Kunde, R.S. Jangid, Effects of pier and deck flexibility on the seismic response of isolated bridges. *Journal of Bridge Engineering*, **11**(1), 109-121, 2006.
- [21] A. Mokha , M.C. Constantinou, A.M. Reinhorn, Teflon Bearings in Base Isolation I: Testing. *J. Struct. Eng.*, **116**(2), 438-454, 1990.
- [22] M.C. Constantinou, A. Mokha, A. M. Reinhorn, Teflon Bearings in Base Isolation II: Modeling. *J. Struct. Eng.*, **116**(2), 455-474, 1990.
- [23] M.C. Constantinou, A.S. Whittaker, Y. Kalpakidis, D.M. Fenz, G.P. Warn, Performance of Seismic Isolation Hardware Under Service and Seismic Loading. *Technical Report*, 2007.
- [24] P. Castaldo, E. Tubaldi, Influence of ground motion characteristics on the optimal single concave sliding bearing properties for base-isolated structures. *Soil Dynamics and Earthquake Engineering*, **104**, 346–364, 2018.
- [25] R.D. Bertero, V.V. Bertero, Performance-based seismic engineering: the need for a reliable conceptual comprehensive approach. *Earthquake Engineering and Structural Dynamics*, **31**, 627–652, 2002.
- [26] N. Shome, C.A. Cornell, P. Bazzurro, J.E. Carballo, Earthquake, records, and nonlinear responses. *Earthquake Spectra*, **14**(3), 469-500,1998.
- [27] P. Castaldo, B. Palazzo, T. Ferrentino T., Seismic reliability-based ductility demand evaluation for inelastic base-isolated structures with friction pendulum devices. *Earthquake Engineering and Structural Dynamics*, **46**(8): 1245-1266, 2017, DOI: 10.1002/eqe.2854.
- [28] Castaldo, P., Palazzo, B., Ferrentino, T., & Petrone, G. (2017). Influence of the strength reduction factor on the seismic reliability of structures with FPS considering intermediate PGA/PGV ratios. *Composites Part B: Engineering*, 115, 308-315.
- [29] Palazzo, B., Castaldo, P., & Della Vecchia, P. (2014, September). Seismic reliability analysis of base-isolated structures with friction pendulum system. In 2014 IEEE Workshop on Environmental, Energy, and Structural Monitoring Systems Proceedings (pp. 1-6). IEEE.
- [30] P. Castaldo, B. Palazzo, G. Alfano, M.F. Palumbo, Seismic reliability-based ductility demand for hardening and softening structures isolated by friction pendulum bearings. *Struc. Control and Health Monitoring*, e2256, 2018.
- [31] H. Aslani, E. Miranda, Probability-based seismic response analysis. *Engin. Structures*, **27**(8), 1151-1163, 2005.
- [32] Garzillo C., Troisi R. Le decisioni dell'EMA nel campo delle medicine umane. In EMA e le relazioni con le Big Pharma - I profili organizzativi della filiera del farmaco, G. Giappichelli, 85-133, 2015.

- [33] De Iuliis, M., & Castaldo, P. (2012). An energy-based approach to the seismic control of one-way asymmetrical structural systems using semi-active devices. *Ingegneria Sismica-International Journal of Earthquake Engineering*, 29(4), 31-42.
- [34] Golzio L. E., Troisi R. The value of interdisciplinary research: a model of interdisciplinarity between legal re-search and research in organizations. *Journal For Development And Leadership*, 2: 23-38, 2013.
- [35] Basone, F., Castaldo, P., Cavaleri, L., & Di Trapani, F. (2019). Response spectrum analysis of frame structures: reliability-based comparison between complete quadratic combination and damping-adjusted combination. *Bulletin of Earthquake Engineering*, 17(5), 2687-2713.
- [36] Nese A., Troisi R. Corruption among mayors: evidence from Italian Court of Cassation judgments, *Trends In Organized Crime*, 1-26, 2018. DOI:10.1007/s12117-018-9349-4.
- [37] Troisi R., Golzio, L. E. Legal studies and organization theory: a possible cooperation. *Manageable cooperation* - European Academy of Management: 16th EURAM Conference, Paris, 1-2, 1-4 June 2016.
- [38] Troisi R., Guida V. Is the Appointee Procedure a Real Selection or a Mere Political Exchange? The Case of the Italian Health-Care Chief Executive Officers. *Journal of Entrepreneurial and Organizational Diversity*, 7 (2): 19-38, 2018, DOI:10.5947/jeod.2018.008.
- [39] Troisi R. Le risorse umane nelle BCC: lavoro e motivazioni al lavoro. In *Progetto aree bianche. Il sistema del credito cooperativo in Campania*, 1: 399-417, 2012.
- [40] A.H.S. Ang, W.H. Tang, Probability Concepts in Engineering-Emphasis on Applications to Civil and Environmental Engineering. *John Wiley & Sons*, New York, USA, 2007.
- [41] Math Works Inc. MATLAB-High Performance Numeric Computation and Visualization Software. *User's Guide*. Natick: MA, USA, 1997.